Desalination and Water Treatment
www.deswater.com

doi: 10.5004/dwt.2017.21752

100 (2017) 160–167
December

Structural study and photocatalytic performance of ZnO thin films prepared by electrochemical deposition

Safeya A. Taha, Alaa M. Abd-Elnaiem*, Mansour Mohamed, Samar Mostafa, M.S. Mostafa

Physics Department, Faculty of Science, Assiut University, 71516 Assiut, Egypt, email: safeya.taha@gmail.com (S.A. Taha), Tel. +20882412229, Fax +20882342708, email: abd-elnaiem@aun.edu.eg (A.M. Abd-Elnaiem), m.mohamed@aun.edu.eg (M. Mohamed), samer.abdelrehem@science.au.edu.eg (S. Mostafa), mostafa.ali1@science.au.edu.eg (M.S. Mostafa)

Received 20 April 2017; Accepted 2 December 2017

ABSTRACT

In this study, zinc oxide (ZnO) thin films were deposited on Fluorine-doped tin oxide (FTO) substrates by electrochemical deposition (ECD) technique. The ECD was carried out at a constant potential over a range of deposition times. The current-time response was recorded and discussed. The crystal structure and morphologies of the films were studied using X-ray diffraction (XRD) and scanning electron microscopy (SEM), respectively. Furthermore, photocatalytic performance of methylene blue using ZnO was investigated at various quantity of ZnO and irradiation time. The photocatalysis results showed the dependence of photodegradation process on the quantity of catalyst and irradiation time. Moreover, the degradation rate constant and adsorption equilibrium constant were calculated. Our analyses indicate that quantity of catalyst affects the degradation rate constant and the efficiency, while the adsorption equilibrium constant does not.

Keywords: ZnO; Electrochemical deposition; Structural; Photocatalysis; Thin film

1. Introduction

Zinc oxide (ZnO) is an n-type semiconductor with broad and direct band gap of 3.37 eV at 300 K, and a large free excitonic binding energy of 60 meV [1–4]. Due to its interesting physicochemical properties, ZnO is suitable for many technological applications such as photovoltaic, environmental remediation, nanoelectronic devices, clean energy production, sensing, and solar cells among others [5,6].

ZnO thin films have been prepared via a number of methods such as sol-gel, radio frequency plasma, pulsed laser deposition, ion-assisted cyclic sputtering, thermal evaporation, electron beam evaporation, spray pyrolysis, chemical vapor deposition, electrochemical deposition (ECD) method, ionic layer adsorption and reaction, among others [1–17]. Of these methods, ECD route is desirable not only because of its simplicity and low cost of deposition equipment but also easier control of the film thickness and morphology. Also, ECD makes fabrication of large-area thin films possible. Generally, the physical and chemical properties of the prepared thin films depend on the fabricating parameters (such as electrolyte type, concentration, pH, and temperature; deposition time; applied potential or current; substrate type, etc) and subsequent heat treatment.

The fabrication and characterization of nanostructures and thin films of electrodeposited ZnO have been extensively studied [1–4,13–22]. For instance, Tayet al. [19] used transmission X-ray microscopy to observe in situ nucleation and growth during electrochemical deposition of ZnO. Similarly, Izaki et al. [3] prepared highly transparent (73%) ZnO films on a conductive substrate by electrochemical reaction method. Elsewhere [4], ZnO films of good quality have been cathodically deposited on NESA glasses from aqueous 0.03 to 0.1 M zinc nitrate electrolyte at 335 K. While Peulon et al. [14] showed that the deposition temperature significantly affects the crystalline state of the prepared ZnO films, Yoshida et al. [15] reported that, in the presence of certain organic molecules, ECD of ZnO thin films results in self-assembly of various hybrid thin films with new properties [15]. Annealing temperatures also influence the crystal structure and hence the material properties such as

*Corresponding author.

luminescence among others [16]. Wange et al. studied the effect of annealing temperature on the structural and optical properties of electrodeposited ZnO [18]. They found that annealing enhanced and sharpened the excitonic emission band and decreased the deep level emission. Moreover, the effect of the electrochemical technique on the crystallinity, morphological and photoelectrochemical properties of ZnO are well documented [20].

The photocatalytic process based semiconducting oxides have received significant attention as environmental friendly, low production cost, and sustainable technology for water purification and splitting [12,17,23]. Advanced oxidation technology has been widely established to remove persistent organic compounds and microorganisms in water [24]. Since reaction occurs at the surface of the photocatalytic layer, any increase in the active surface area or changes in the structural geometry, band gap, stability and reusability of the oxide would optimize the degradation performance. In a similar vein, ZnO has been extensively used as heterogeneous photocatalysts [25]. This could be attributed to its stability, biocompatibility, and ability to generate charge carriers when stimulated with the desired amount of energy. The photocatalytic process is usually obliged for the purification of waste water, by eliminating harmful bacteria and other pollutants, as this can render water reusable.

In this work, ZnO thin films were deposited on Fluorine-doped tin oxide (FTO) substrate using ECD technique. The films were characterized with X-ray diffraction (XRD) and scanning electron microscope (SEM). The effects of deposition time on the structure and morphology of the films are discussed. Furthermore, the effect of ZnO quantity and irradiation time on the photocatalytic performance are examined.

2. Materials and methods

2.1. Materials

Zinc nitrate, $Zn(NO_3)_2$ and methylene blue (MB) dye, $C_{16}H_{18}ClN_3S$, were purchased from Sigma-Aldrich Chemicals. They were used as received without further purification. All aqueous solutions were prepared using double distilled water.

2.2. Preparation and structural analysis of ZnO

ZnO thin films were synthesized by the cathodic potentiostatic ECD method. The ECD process was performed using a three-electrode cell configuration consisting of a working electrode (WE), a reference electrode (RE) and a counter electrode (CE). In all our experiments, Ag/AgCl electrode in saturated KCl solution was used as RE and an inert platinum wire was used as CE. The FTO glass substrate with a rectangular area of 1.5 cm^2 was used as WE. $Zn(NO_3)_2$ with concentration 0.1 M was used for the ZnO deposition at 327 K for three different durations: 10, 30, and 60 min. Prior to the deposition, the FTO substrate was ultrasonically cleaned in ethanol and deionized water for 10 min and then dried in air. A constant potential, –1 V, was applied during the deposition. The potential was well controlled and the current responses were recorded via Autolab PGSTAT101 using NOVA electrochemical software. Thereafter, the samples were rinsed carefully with deionized water and then dried in air.

The phase and crystal structure of the ZnO films were investigated with Philips X-ray diffractometer (type-1710) operated at 40 kV and 40 mA with monochromatic Cu kα radiation (λ = 1.5418 Å). The 2θ values of the diffracted beams were scanned in the range of 15°–90° at a scan rate of ~0.06 degree/s. The XRD patterns were fitted with Igor (version: 6.22A) from where the full-width-at-half-maximum (FWHM) values were obtained. The morphology of ZnO films was examined by using a SEM (Model JOEL-JSM-5400LV) operated at 15 kV. A Java image processing software (ImageJ, Version 1.37) was used to determine the porosity of the film based on SEM images.

2.3. Photocatalytic activity measurement

In the photocatalytic experiment, different amounts of the as-prepared ZnO (without FTO substrate) samples, 0, 0.5, 1 and 2 g/L were dispersed in 10^{-5} M MB dye. The experiments were carried out in a Pyrex reactor and an artificial Sunlight Simulator of 450 W/m^2 (Model Oriel SO12A). Solar Simulator was associated with an ultraviolet filter. The degradation of organic dye was monitored by measuring the changes in the UV-Vis absorption spectra as a function of irradiation time. The spectra were measured using Lambda 750 UV-Vis spectrophotometer with a scanning rate of 3 nm/s. The degradation process was examined for a period of 150 min.

The photocatalytic efficiency (η) or removal efficiency of MB was evaluated from Eq. (1) [27]:

$$\eta(\%) = \frac{C_0 - C_t}{C_0} \times 100 = \frac{A_0 - A_t}{A_0} \times 100 \quad (1)$$

where C_0 is the initial dye concentration and C_t the residual dye concentration after irradiation time (t). The absorbance A_0 is corresponding to the concentration C_0 of the solution and the absorbance A_t measured after variable periods of irradiation was taken as corresponding to the residual concentration C_t.

3. Results and discussion

3.1. Characterization of ZnO films

3.1.1. Current-time transient curves

Fig. 1 shows the current density-time (j-t) curve obtained during the ECD of ZnO at 327 K. The applied potential (–1 V) was chosen to avoid the reduction of Zn^{+2} and the formation of metallic zinc phase [1]. The duration of deposition changed from 10 min as observed in Fig. 1a to 1 h in Fig. 1b in order to obtain different film thicknesses. The behavior of j-t curve can be divided into three stages. In the initial stage (stage-I), the current density drops from the highest value (–3.9 mA cm^{-2}) to a minimum value (–2.59 mA cm^{-2}) (Fig. 1a). The observed drop in current density is attributed to the induction process (the charge-discharge process of double layer) at FTO/electrolyte interface. The approximated dura-

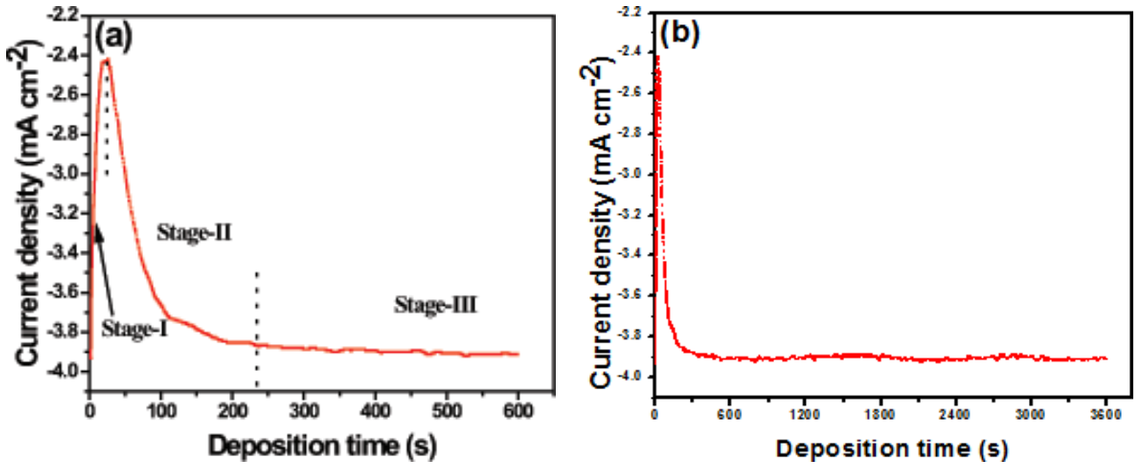

Fig. 1. *j-t* curves obtained during the electrochemical deposition of ZnO from 0.1 M $Zn(NO_3)_2$ at –1 V and 327 K for (a) 10 min and (b) 60 min.

tion for this stage is about 22 s. In the second stage (stage-II), the current density increases to a stable value, 3.87 mA cm^{-2}, which corresponds to the increase of active surface area for the ECD process. This increase might be attributed to the instantaneous and three-dimensional growth of ZnO crystal. The third stage (stage-III) is characterized by constant current density deposition due to the steady-state growth of the film.

The ECD process of ZnO thin films from nitrate solution can be described by the following Eqs. (2)–(5):

$$Zn(NO_3)_2 \rightleftarrows Zn^{2+} + 2NO_3^- \quad (2)$$

$$NO_3^- + H_2O + 2e \rightleftarrows NO_2^- + 2OH^- \quad (3)$$

$$Zn^{2+} + 2OH^- \rightleftarrows Zn(OH)_2 \quad (4)$$

$$Zn(OH)_2 \rightleftarrows ZnO + H_2O \quad (5)$$

The corresponding thickness, *d*, can be estimated using the well-known Faraday's law:

$$d = \frac{M}{nFA}Q \quad (6)$$

where *n* is the number of transferred electrons which is considered to be 2, *F* is Faraday's constant (9.6×10^4 C/mol), *Q* is the consumed charge during the ECD process, *A* is the exposed area for electrodeposition which is adjusted to be 1.5 cm^2, and *M* is the molar mass of ZnO (81.408 g/mol). The values of charge consumed during deposition are 1.27, 6.93, and 13.7 C/cm^2 for 10, 30 and 60 min, respectively. The estimated thicknesses of ZnO are 0.6, 3.3, and 6.5 μm, respectively. As expected, the thickness of ZnO increased with deposition time. It should be noted that these calculations were utilized for the dense (nonporous) ZnO thin films. For both porous and nonporous thin films, an alternative method is discussed in the following section.

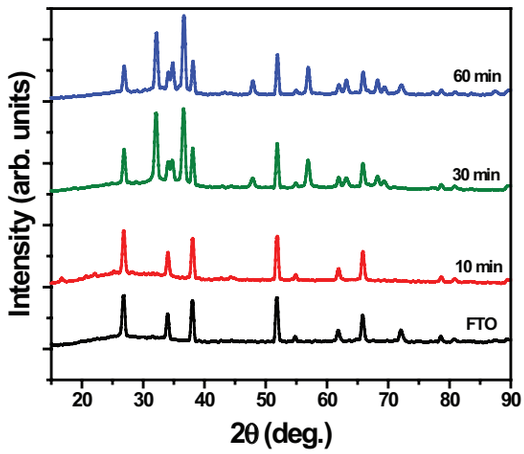

Fig. 2. XRD patterns for FTO substrate and the electrodeposited ZnO films on FTO substrate prepared at a different deposition time of 10, 30 and 60 min.

3.1.2. Crystal structure analysis

To identify the crystalline nature of the films, the XRD patterns of the FTO substrate was subtracted from those of the electrodeposited ZnO-on-FTO films for all the deposition periods (Fig. 2). The analysis of the XRD patterns for all ZnO samples reveal the coexistence of the hexagonal ZnO phase (ICDD database, File:00-050-0792). Miller indices at the planes (002), (101), (102), (110), (103) and (112), which correspond to the diffraction angle (2θ) of 34.7, 36.58, 47.9, 56.9, 63.15 and 68.26°, show hcp structure. It can be seen that electrodeposited ZnO films show sharp peak at 2θ = 36.58°, suggesting that the growth is along a-, and c-axes. This is attributed to the growth at temperature lower than 343 K; however, the high-quality c-axis oriented ZnO films can be prepared at 343 K [28]. Usually, the formation of ZnO by ECD is preferably at high temperature (≥343 K), however flower-like porous and nanosphere ZnO are prepared at lower temperatures (333 K and 313 K). Unfortunately, the growth of ZnO at higher tempera-

ture leads to faster diffusion with subsequent large crystal [29]. It can be seen that the intensity and the FWHM of the observed peaks are dependent on the deposition time. However, the growth prefers orientation remain normal to the FTO substrate. The average crystallite size D_{hkl} of the hexagonal ZnO phase for the as-prepared samples along a certain plane of crystalline material was calculated from the XRD patterns according to well-known Scherrer's equation [26]:

$$D_{hkl} = \frac{k\lambda}{\beta_{hkl}\cos(\theta)} \tag{7}$$

where k is the Scherrer's constant (generally taken as one), its value is related to the particle shape, θ is the Bragg angle, λ is the wavelength and β_{hkl} is the FWHM of the powder reflection peak. The deduced values of D_{hkl} corresponding Miller indices and other structures parameters are listed in Table 1. It is evident that the average crystallite size of the films slightly increases from 16.77 nm to 19.18 nm as deposition time increases from 30 min to 60 min. Also, the intensity increases as the deposition time increases. Accordingly, it is, difficult to see any ZnO peak for the deposition time of 10 min which might be attributed to the small amount of ZnO being deposited.

The inter-planar spacing, d_{hkl}, and lattice constants a and c of hexagonal structure of ZnO were estimated by the following equations:

$$d_{hkl} = \frac{\lambda}{2\sin(\theta)} \tag{8}$$

$$a = \frac{\lambda}{2\sin(\theta)}\sqrt{\frac{4}{3}\left(h^2 + hk + \frac{l^2}{(c/a)^2}\right)} \tag{9}$$

$$c = \frac{\lambda}{2\sin(\theta)}\sqrt{\frac{4}{3(a/c)^2}\left(h^2 + hk + l^2\right)} \tag{10}$$

The estimated values of the structural parameters are summarized in Table 1.

3.1.3. Microstructure of the prepared ZnO

The deposition time is one of the most important parameters that influence the surface morphology of materials. The top-view and cross-section SEM images of ZnO thin films (Fig. 3) reveal porous microstructure, the quantity of which depends on the disposition time. For the ZnO film deposited after 10 min, small thickness and nanosheets shape are well observed (Fig. 3b). However, with increased deposition time, the thickness of these nanosheets/nanoplates increases, and the nanosheets shape becomes more complicated (Fig. 3c). After 60 min, thicker ZnO film with nested stick shape was obtained (Fig. 3d). This implies the formation of the greater surface area that could help in absorption process during photocatalytic degradation. The nanosheet wall thickness increased from 80±10 nm to 130±20 nm as the deposition time changes from 10 min to 60 min, respectively. This is in agreement with calculated values based on Faraday's law. While the increased deposition time does not significantly affect the crystallinity, its effect on the film morphology is largely pronounced. These observations are in good agreement with several studies [19,21,22,30]. The exact thickness of porous ZnO samples was estimated using SEM images (Figs. 3e, f). The values are 7.04±0.5 and 20.5±3.9 μm for deposition time of 30 and 60 min, respectively. The deviation between the theoretical (estimated from Faraday's law) and experimental thickness (estimated from SEM images) values could be attributed to the high porosity of the prepared films. The density of ZnO changes from 5.6 g/cm^3 to 2.62 and 1.77 g/cm^3 corresponding to samples prepared for 30 min and 60 min, respectively. Thereafter, the porosity (P) of porous ZnO films was also calculated from the density of dense (ρ_d = 5.6 g/cm^3) and porous (ρ_p) ZnO using Eq. (11):

$$P(\%) = \left(1 - \frac{\rho_P}{\rho_d}\right) \times 100 \tag{11}$$

The porosity of ZnO changes from 53 to 68.3 % as electro depositing time changes from 30 to 60 min, respectively. The higher porosity is expected to play an import-

Table 1
Structural parameters of the prepared ZnO films

Duration	2θ	34.06	36.58	47.89	56.92	63.16	68.25	Average Crystallite size (nm)
30 min	Plane	(002)	(101)	(102)	(110)	(103)	(112)	16.77
	d_{hkl} (nm)	0.263	0.245	0.190	0.161	0.147	0.137	
	a (nm)	0.430	0.384	0.401	0.305	0.411	0.343	
	c (nm)	0.990	0.653	0.799	0.430	0.875	0.633	
	D_{hkl} (nm)	19.05	16.31	14.20	16.73	15.01	19.35	
60 min	2θ	34.06	36.64	47.89	56.94	63.16	68.26	19.18
	Plane	(002)	(101)	(102)	(110)	(103)	(112)	
	d_{hkl} (nm)	0.263	0.245	0.190	0.162	0.147	0.137	
	a (nm)	0.430	0.383	0.401	0.305	0.411	0.343	
	c (nm)	0.990	0.652	0.799	0.430	0.875	0.237	
	D_{hkl} (nm)	–	17.44	18.56	19.30	18.83	21.93	

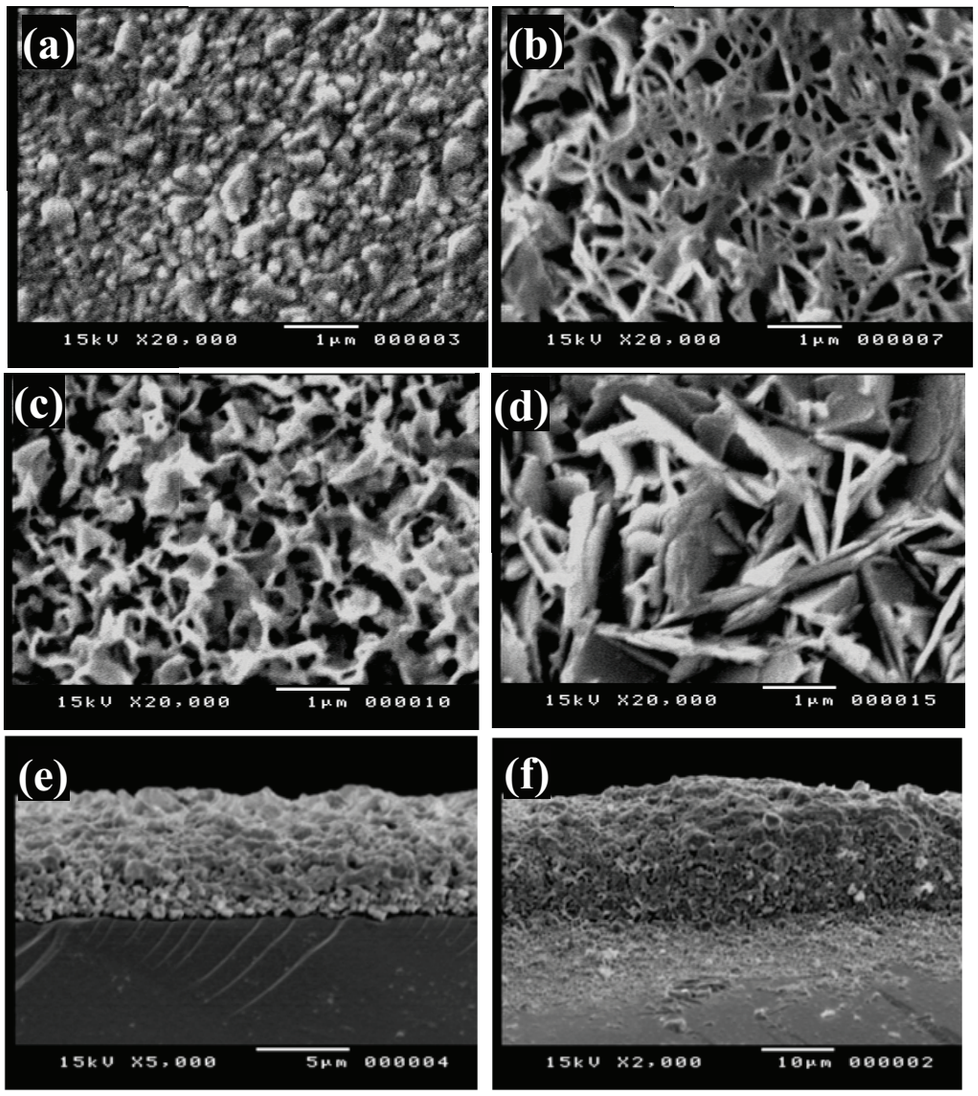

Fig. 3. SEM images show top-view of (a) FTO glass substrate before ECD of ZnO, ZnO/FTO after deposition of ZnO for (b) 10 min, (c) 30 min, and (d) 60 min, and cross-section images for ZnO prepared by ECD for (e) 30 min, and (f) 60 min.

ant role in the applications which requires higher surface area such as water purification process and energy storage applications.

3.2. Photocatalytic activity of porous ZnO films

It should be noted that MB was used as an arbitrary dye in our present study. There are many conditions which could affect the photocatalytic degradation of MB using ZnO as a catalyst. Among them are the electrolyte pH, irradiation time, the amount of catalyst and initial dye concentration. These conditions were taken into account to achieve the integrated model for the photocatalytic degradation of MB.

First, the Lambert-Beer correlation was plotted to determine the linear relation between absorbance and dye concentration. Second, photocatalytic performances of ZnO samples were recorded by measuring the absorbance for different durations of UV irradiation. The absorbance values (α) were converted to molarities (C), or vice versa, based on Eq. (12):

$$\alpha = ebC \tag{12}$$

where e is the molar absorptivity with units of L/mol·cm, and b is the path length of the sample in centimeters. According to our estimations, this relation can be written as:

$$\alpha = 6.05 \times 10^5 C \tag{13}$$

This function will be used for the molarity estimation of the degraded MB solutions. It is important to note that the measured maximum absorbance values at 664 nm wavelength (absorbance peak) at different irradiation time from

0 to 150 min were converted to molarities using Eq. (13). The values of absorbance and the corresponding residual concentration (C_t) are summarized in Table 2.

3.2.1. Effect of irradiation time

The effect of irradiation time on the photodegradation efficiency of MB was studied by measuring the absorbance at different period up to 150 min for the various quantity of ZnO catalyst 0.5, 1 and 2 g/L in MB at room temperature (303 K). In the absence of photocatalytic; the degradation of dye is too weak, and therefore can be neglected. For simplicity, samples were denoted as sample 1, 2 & 3 corresponding to 0.5, 1 and 2 g/L, respectively. One can observe a maximum peak at 644 nm for these samples (Fig. 4). Furthermore, the absorbance decreases with increased irradiation time, resulting in a reduction in the concentration of MB. The results in Table 2 indicate that the degradation efficiency increases with increased irradiation time. The observed decrease in MB absorbance of light and concentrations can be attributed to the degradation process (Fig. 4). These results show that the photocatalytic activity increases with increased irradiation time. The results also confirmed that the relatively high activity of the prepared catalysts indicates that the catalysts have active reaction sites. The relative concentrations of MB (C/C_0) decreased with the irradiation time (Fig. 5).

3.2.2. Effect of catalyst amount

The amount of ZnO, catalyst significantly affects the photodegradation efficiency of MB [27]. In our case, this effect was observed for the quality range of 0.5–2 g/L in 50 ppm dye solution under visible light at room temperature for constant irradiation time (150 min). The results obtained (Table 2) revealed that as the quantity of catalyst changed from 0.5 to 2 g/L, the photodegradation efficiency of MB increased from 38 to 60.4%. This could be attributed to the increased number of available active sites on the catalyst reaction surface, thereby increasing the number of holes and hydroxyl radicals. The values of absorbance, residual concentration, and photodegradation efficiency as a function of the amount of ZnO as a catalyst are listed in Table 2.

3.2.3. Photocatalytic kinetics

The photodegradation of MB (C_0 = 10 μM) can be considered as a pseudo-first-order kinetic reaction. Therefore, photocatalytic kinetics parameters such as the adsorption equilibrium constant (K) and degradation rate constant (k) are determined according to Eq. (14) [24,31]:

$$\ln\left(\frac{C}{C_0}\right) = -kKt + KC_0\left(1-\frac{C}{C_0}\right) \tag{14}$$

For example, for sample 1 (m = 0.5 g/L), for different irradiation times Eq. (14) can be written as:

$$\left.\begin{aligned} -0.17 &= -20kK + 1.32\times10^{-6}K \\ -0.23 &= -40kK + 1.63\times10^{-6}K \\ -0.27 &= -60kK + 1.83\times10^{-6}K \\ -0.34 &= -90kK + 2.06\times10^{-6}K \\ -0.39 &= -120kK + 2.18\times10^{-6}K \\ -0.47 &= -150kK + 2.35\times10^{-6}K \end{aligned}\right\} \tag{15}$$

The average values of K and k, calculated by solving Eq. (15), are listed in Table 2. This procedure is repeated for

Table 2
Photocatalytic parameters of ZnO for different conditions

Photocatalytic parameter	ZnO amount (g/L)	Irradiation time (min)					
		20	40	60	90	120	150
Absorbance	0.5	0.511	0.482	0.46	0.43	0.411	0.378
Residual concentration C_t (M)		8.4×10^{-6}	7.9×10^{-7}	7.6×10^{-6}	7.1×10^{-6}	6.8×10^{-6}	6.25×10^{-6}
Efficiency (%)		16	20.5	24.1	29	32.2	38
Degradation rate constant k (M/min)		1.1×10^{-8}					
Adsorption equilibrium constant K (/M)		-1.1×10^{5}					
Absorbance	1	0.404	0.40	0.39	0.37	0.35	0.33
Residual concentration C_t (M)		6.67×10^{-6}	6.6×10^{-6}	6.4×10^{-6}	6.1×10^{-6}	5.8×10^{-6}	5.5×10^{-6}
Efficiency (%)		33.3	34	35.6	38.9	42.2	45.5
Degradation rate constant k (M/min)		1.3×10^{-8}					
Adsorption equilibrium constant K (/M)		-1.3×10^{5}					
Absorbance	2	0.33	0.329	0.31	0.288	0.26	0.24
Residual concentration C_t (M)		5.45×10^{-6}	5.44×10^{-6}	5.12×10^{-6}	4.75×10^{-6}	4.3×10^{-6}	3.97×10^{-6}
Efficiency (%)		45.5	45.7	48.8	52.4	57	60.4
Degradation rate constant k (M/min)		1.6×10^{-8}					
Adsorption equilibrium constant K (/M)		-1.9×10^{5}					

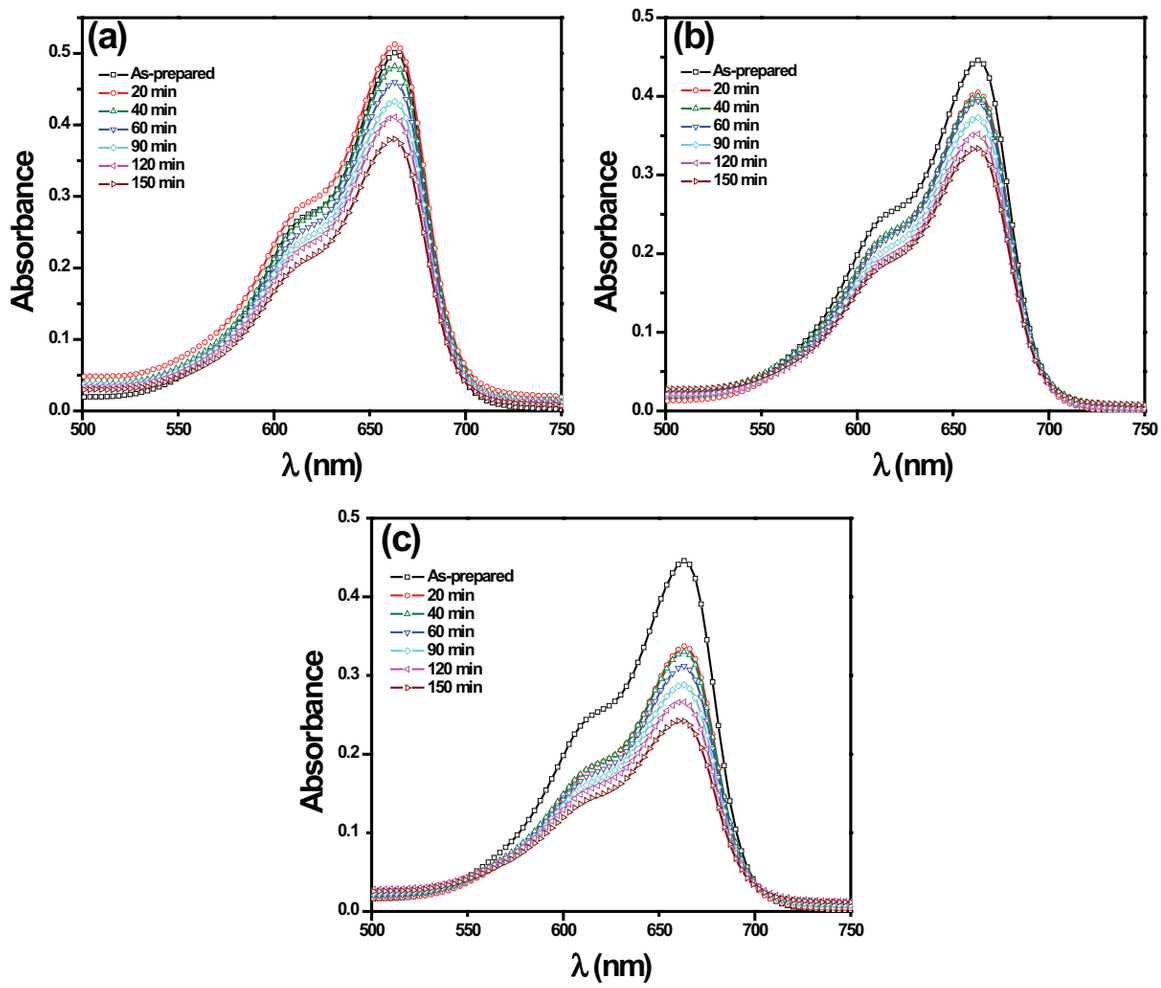

Fig. 4. The main photocatalytic peak for ZnO sample in MB using different amounts of ZnO in MB (a) 0.5 g/L, (b) 1 g/L, (c) 2 g/L.

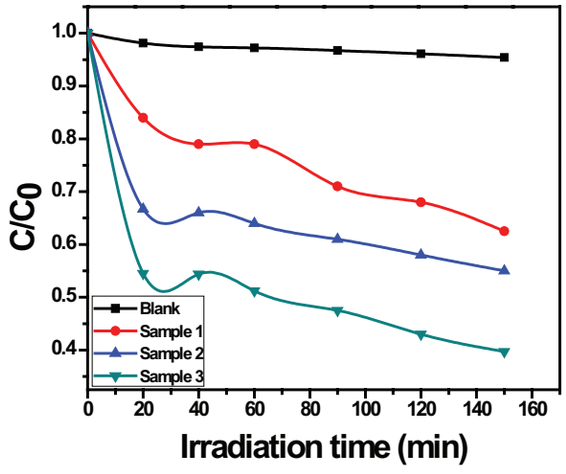

Fig. 5. Variation of the relative concentration of MB (C/C_0) versus the irradiation time for the three samples. Black squares curve represent the MB solution without catalysts under the light irradiation.

other samples. Table 2 shows that the efficiency increases with increased irradiation time as well the quantity of catalyst. Both the adsorption equilibrium constant and degradation rate constant were not affected by the increased irradiation time.

Generally, the degradation mechanism has been explored and reported [32]. The exposure of ZnO to UV radiation leads to a generation of electron-hole pairs, which can react with water to produce hydroxyl and superoxide radicals. Then the radicals initiate a series of chemical reactions and act as a strong oxidizing agent to mineralize the pollutants such as MB. Then, the higher surface area of ZnO nanostructures results in higher adsorption of MB at the same amount of catalyst and irradiation time. The great surface area and adsorption ability of the hybrid film not only support the interactions between the catalyst and dye but also supply more active sites which are suitable for the generation of hydroxyl radicals. This implies that MB is capable of filling the self-tailored space subtly and exclusively. The photodegradation efficiency is drastically enhanced with increased irradiation time and amount of ZnO in wastewater.

4. Conclusions

We studied the structural and morphology properties of ZnO film prepared by ECD technique and investigated the photocatalytic activity of the product. Characterization of ZnO nanostructures was realized using XRD and SEM. The XRD results showed that the nanocrystalline ZnO with a hexagonal structure and small crystallite size can be prepared by ECD method at 327 K. In addition, the SEM images revealed that the surface morphology of ZnO films depends greatly on the deposition time. Similarly, photocatalytic performance of MB showed that higher quantity of ZnO enhances photodegradation process. Thus, the ZnO nanostructured semiconductor prepared by ECD can play a major role in photocatalytic applications and could be used as alternative low cost and environmentally friendly solution for water purification.

References

[1] A. Kathalingam, M.R. Kim, Y.S. Chae, J.K. Rhee, T. Mahalingam, Studies on electrochemically deposited ZnO thin films, J. Korean Phys. Soc., 55 (2009) 2476–2481.

[2] A. Kołodziejczak-Radzimska, T. Jesionowski, Zinc oxide—from synthesis to application: a review, Materials, 7 (2014) 2833–2881.

[3] M. Izaki, T. Omi, Transparent zinc oxide films prepared by electrochemical reaction, Appl. Phys. Lett., 68 (1996) 2439–2440.

[4] M. Izaki, Takashi Omi, Electrolyte optimization for cathodic growth of zinc oxide films, J. Electrochem. Soc., 143 (1996) L53–L55.

[5] A. Raidou, M. Aggour, A. Qachaou, L. Lanab, M. Fahoume, Preparation and characterization of ZnO thin films deposited by SILAR method, MJ Condens. Matter, 12 (2010) 125–130.

[6] S.G. Kumar, K.K. Rao, Zinc oxide based photocatalysis: tailoring surface-bulk structure and related interfacial charge carrier dynamics for better environmental applications, RSC Adv., 5 (2015) 3306–3351.

[7] Y.T. Chung, M.M. Ba-Abbad, A.W. Mohammad, A. Benamor, Functionalization of zinc oxide (ZnO) nanoparticles and its effects on polysulfone-ZnO membranes, Desal. Water Treat., 57(17) (2016) 7801–7811.

[8] P. Murkute, H. Ghadi, S. Saha, S.K. Pandey, S. Chakrabarti, Enhancement in optical characteristics of c-axis-oriented radio frequency–sputtered ZnO thin films through growth ambient and annealing temperature optimization, Mat. Sci. Semicon. Proc., 66 (2017) 1–8.

[9] A. Zawadzka, P. Płóciennik, Y. El Kouari, H. Bougharraf, B. Sahraoui, Linear and nonlinear optical properties of ZnO thin films deposited by pulsed laser deposition, J. Lumin., 169 (2016) 483–491.

[10] H. Belkhalfa, H. Ayed, A. Hafdallah, M.S. Aida, R.T. Ighil, Characterization and studying of ZnO thin films deposited by spray pyrolysis: effect of annealing temperature, Optik, 127(4) (2016) 2336–2340.

[11] S.A. Gawali, S.A. Mahadik, F. Pedraza, C.H. Bhosale, H.M. Pathan, S.R. Jadkar, Synthesis of zinc oxide nanorods from chemical bath deposition at different pH solutions and impact on their surface properties, J. Alloy. Compd., 704 (2017) 788–794.

[12] M. Rashad, N.M. Shaalan, A.M. Abd-Elnaiem, Degradation enhancement of methylene blue on ZnO nanocombs synthesized by thermal evaporation technique, Desal. Water Treat., 57 (2016) 26267–26273.

[13] D. Chu, S. Li, Growth and electrical properties of doped ZnO by electrochemical deposition, New J. Glass Ceram., 2 (2012) 13–16.

[14] S. Peulon D. Lincot, Mechanistic study of cathodic electrodeposition of zinc oxide and zinc hydroxychloride films from oxygenated aqueous zinc chloride solutions, J. Electrochem. Soc., 145 (1998) 864–874.

[15] T. Yoshida, J. Zhang, D. Komatsu, S. Sawatani, H. Minoura, T. Pauporté, D. Lincot, T. Oekermann, D. Schlettwein, H. Tada, D. Wöhrle, Electrodeposition of inorganic/organic hybrid thin films, Adv. Funct. Mater., 19 (2009) 17–43.

[16] T. Pauporte, D. Lincot, Heteroepitaxial electrodeposition of zinc oxide films on gallium nitride, Appl. Phys. Lett., 75 (1999) 3817–3819.

[17] P. Liu, W. Li, J. Zhang, Electrodeposition and photocatalytic selectivity of ZnO/methyl blue hybrid thin films, J. Phys. Chem. C, 113 (2009) 14279–14284.

[18] Q. Wang, G. Wang, J. Jie, X. Han, B. Xu, J.G. Hou, Annealing effect on optical properties of ZnO films fabricated by cathodic electrodeposition, Thin Solid Films, 492 (2005) 61–65.

[19] S.E.R. Tay, A.E. Goode, J. Nelson Weker, A.A. Cruickshank, S. Heutz, A.E. Porter, M.P. Ryan, M.F. Toney, Direct in situ observation of ZnO nucleation and growth via transmission X-ray microscopy, Nanoscale, 8 (2016) 1849–1853.

[20] H. Chettah, D. Abdi, Effect of the electrochemical technique on nanocrystalline ZnO electrodeposition, its structural, morphological and photoelectrochemical properties, Thin Solid Films, 537 (2013) 119–123.

[21] Q. Hou, L. Zhu, H. Chen, H. Liu, W. Li, Growth of flower-like porous ZnO nanosheets by electrodeposition with $Zn_5(OH)_8(NO_3)_2 2H_2O$ as precursor, Electrochim. Acta, 78 (2012) 55–64.

[22] J. Yang, Y. Wang, J. Kong, H. Jia, Z. Wang, Synthesis of ZnO nanosheets via electrodeposition method and their optical properties, growth mechanism, Opt. Mater., 46 (2015) 179–185.

[23] T. Tan, Y. Li, Y. Liu, B. Wang, X. Song, E. Li, H. Wang, H. Yan, Two-step preparation of Ag/tetrapod-like ZnO with photocatalytic activity by thermal evaporation and sputtering, Mater. Chem. Phys., 111 (2008) 305–308.

[24] I. El Saliby, L. Erdei, J.H. Kim, H.K. Shon, Adsorption and photocatalytic degradation of methylene blue over hydrogen–titanate nanofibres produced by a peroxide method, Water Res., 47 (2013) 4115–4125.

[25] M. El Hajji, A. Hallaoui, L. Bazzi, A. Benlhachemi, O. Jbara, A. Tara, B. Bakiz, Nanostructured ZnO, ZnO-CeO_2, ZnO-Cu_2O thin films electrodes prepared by electrodeposition for electrochemical degradation of dye, Int. J. Electrochem. Sci., 9 (2014) 4297–4314.

[26] U. Holzwarth, N. Gibson, The Scherrer equation versus the Debye-Scherrer equation, Nat. Nanotechnol., 6 (2011) 534–534.

[27] R.M. Mohamed, I.A. Mkhalid, E.S. Baeissa, M.A. Al-Rayyani, Photocatalytic degradation of Methylene Blue by Fe/ZnO/SiO_2nanoparticles under visible light, J. Nanotech., 2012 (2012) 1–5.

[28] S. Otani, J. Katayama, H. Umemoto, M. Matsuoka, Effect of bath temperature on the electrodeposition mechanism of zinc oxide film from zinc nitrate solution, J. Electrochem. Soc., 153(8) (2006) C551–C556.

[29] D. Chu, T. Hamada, K. Kato, Y. Masuda, Growth and electrical properties of ZnO films prepared by chemical bath deposition method, Phys. Status Solidi A, 206(4) (2009) 718–723.

[30] X. Li, S. Cheng, S. Deng, X. Wei, J. Zhu, Q. Chen, Direct observation of the layer-by-layer growth of ZnO nanopillar by in situ high resolution transmission electron microscopy, Sci. Rep., 7 (2017) 40911–40919.

[31] H. Yan, J. Hou, Z. Fu, B. Yang, P. Yang, K. Liu, M. Wen, Y. Chen, S. Fu, F. Li, Growth and photocatalytic properties of one-dimensional ZnO nanostructures prepared by thermal evaporation, Mater. Res. Bull., 44 (2009) 1954–1958.

[32] X. Li, D. Wang, G. Cheng, Q. Luo, J. An, Y. Wang, Preparation of polyaniline-modified TiO_2 nanoparticles and their photocatalytic activity under visible light illumination, Appl. Catal. B-Environ., 81 (2008) 267–273.